Saddle-splay elasticity of nematic structures confined to a cylindrical capillary

S. Kralj[1,2] and S. Žumer[2]
[1]Faculty of Education, Department of Physics, University of Maribor, Koroška 160, 62000 Maribor, Slovenia
[2]Department of Physics, University of Ljubljana, Jadranska 19, 61000 Ljubljana, Slovenia
(Received 9 May 1994; revised manuscript received 12 August 1994)

The stability of nematic structures within a cylindrical capillary whose wall exhibits a homeotropic boundary condition is studied. The structures are obtained numerically from Euler-Lagrange equations resulting from the minimization of the Frank free energy functional. Stability diagrams are presented showing dependence on elastic properties, surface anchoring, and external transversal field strength. Emphasis is given to the effects of the saddle-splay elastic constant (K_{24}), which plays an important role in the weak anchoring regime. A new structure—the planar polar structure with two line defects—is predicted. It is shown that it is stable in a finite interval of the external field strength in the strong anchoring regime.

PACS number(s): 61.30.Eb, 61.30.Jf, 64.70.Md

I. INTRODUCTION

Liquid crystals in restricted geometries have been the subject of intense research for years. They exhibit a rich variety of qualitatively different structures [1–3] whose stability depends on competition among the bulk elastic, surface, and external field forces. Transition among various structures can be induced by (i) an external field (a so-called Fréedericksz-like structural transition), (ii) changing surface conditions (surface driven structural transition), (iii) changing the shape and size of the cavity (geometrically driven structural transition), and (iv) varying elastic properties, i.e., what is conventionally achieved by temperature variation (temperature driven structural transition).

These structures experience in general significantly different electro-optic properties [4–11], which makes them suitable for various electro-optic applications. Study of confined liquid crystals is also interesting for fundamental physics of finite size systems [12–16], surfaces [17], defects [18], etc. For instance, defects in liquid crystals where orientational order is not uniquely defined are related to defects in seemingly completely different systems whose order parameter has similar symmetry properties [18–22].

The nematic [23,24] phase is the simplest liquid crystal phase. A nematic structure confined to a cavity is in most cases well presented with the uniaxial director field $\mathbf{n}(\mathbf{r})$ and the orientational order parameter $S(\mathbf{r})$. The unit vector field $\mathbf{n}(\mathbf{r})$ describes a local average orientation of a long axis of the nematic molecule while $S(\mathbf{r})$ measures the amount of fluctuations about $\mathbf{n}(\mathbf{r})$. Deviations of $S(\mathbf{r})$ from its value S_b in the undistorted bulk phase can be significant at a liquid crystal boundary and at a defect site. They typically persist from the origin of a perturbation over a size given by the nematic coherence length [24] ξ_n. For conventional nematics even close to the nematic-isotropic transition temperature T_{NI} the coherence length does not much exceed ≈ 10 nm. Therefore in supramicrometer cavities the nematic structure is in most cases well described with the director field alone.

The nematic-substrate interfacial coupling [17] is the most important factor determining ordering in curved geometries. Its anisotropic part, which affects the director orientation, is conventionally called the anchoring interaction. The director orientation which locally minimizes the anchoring free energy contribution is referred to as the easy axis $\mathbf{e}_s$. The cases most often studied involve homeotropic anchoring, where $\mathbf{e}_s$ points along the interface normal $\boldsymbol{\nu}$, and planar anchoring, where $\mathbf{e}_s$ is perpendicular to $\boldsymbol{\nu}$.

A lot of studies have been devoted to liquid crystals confined to the cylindrical environment [1,10,11,25–31]. Various structures have been reported for a given anchoring condition. In the following we limit the consideration to the case of homeotropic anchoring. The planar radial [25] with a line defect (PR), the escaped radial [26,27] (ER), and the escaped radial structure with point defects [28] (ERPD) were first theoretically analyzed and observed by optic studies. Cladis and Kleman [26] as well as Meyer [27] showed that the PR structure is realized in cylinders of relatively small radia ($R < 1$ μm). For larger radia they predict stability of the ER or ERPD director field. Later studies using the deuterium NMR enabled one to study nematic patterns in cylinders of submicrometer radia [1,30,31]. These studies have revealed the existence of the planar polar [1] (PP) structure.

Let us first briefly describe the main characteristics of these structures, which are shown in Fig. 1. In the PR structure [Fig. 1(a)] the director field $\mathbf{n}(\mathbf{r})$ has only a radial component with a line defect of strength 1 [18] running along the cylinder axis. The line defect is topologically unstable. Namely, a liquid crystal can avoid this singularity by escaping $\mathbf{n}(\mathbf{r})$ along the cylinder axis. This is realized in the ER structure [Fig. 1(b)]. Due to surface irregularities and intrinsic fluctuations near the nematic-isotropic phase transition the ER structure is often replaced by a more energetic, metastable ERPD configuration [Fig. 1(c)]. It consists of partially escaped domains with alternating radial and hyperbolic point de-

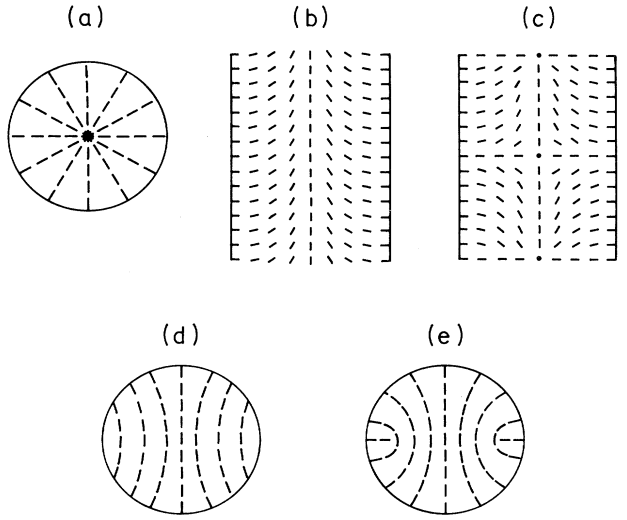

FIG. 1. Schematic representation of a director field of the (a) planar radial (PR), (b) escaped radial (ER), (c) escaped radial with point defects (ERPD), (d) planar polar (PP), and (e) planar polar structure with two line defects (PPLD). Cases (a), (d), and (e): the $(\mathbf{e}_\rho,\mathbf{e}_\varphi)$ plane; cases (b) and (c): the $(\mathbf{e}_\rho,\mathbf{e}_z)$ plane.

fects frozen in. In these "radial-like" structures the director field $\mathbf{n}(\mathbf{r})$ is entirely confined to the $(\mathbf{e}_\rho,\mathbf{e}_z)$ plane in the absence of an external field breaking the cylindrical symmetry of the problem. Here $(\mathbf{e}_\rho,\mathbf{e}_\varphi,\mathbf{e}_z)$ denote the unit vectors of the cylindrical coordinate system.

In another class of structures—"polar-like" structures—the director field is restricted to the $(\mathbf{e}_\rho,\mathbf{e}_\varphi)$ plane with a strong component in the $\mathbf{e}_\varphi$ direction. In the PP structure [Fig. 1(c)] $\mathbf{n}(\mathbf{r})$ tends to be parallel at the cylinder axis and radial at the cylinder wall. The analogy between nematic structures in a cylindrical capillary and spherical droplets [2,32] suggests the possible existence of a planar polar structure with two line defects (PPLD), shown in Fig. 1(e). This structure has two symmetrically running line defects of strength $\frac{1}{2}$ parallel to the cylinder axis.

Recent studies [1,10,11,30,31] have shown that details of these structures and transitions among them clearly reveal elastic and anchoring properties of nematics. Allender and co-workers [1] determined the saddle splay nematic elastic constant K_{24} using the deuterium NMR from (i) details of the ERPD structure and from (ii) the PP-ERPD coexistence point. Later Polak *et al.* [11] measured K_{24} and the surface anchoring strength by studying details of the ER structure with optic polarization microscopy. In addition, Sharkowski *et al.* [10] proposed a new, relatively nondemanding method to measure the ratio of the bend to the splay nematic elastic constant via interference textures of the ER structure.

In those studies the influence of the splay-bend elastic constant K_{13} on nematic structures was neglected. The reason for this is some still not completely resolved mathematical difficulties that the K_{13} term introduces. Recent experimental and theoretical studies [33–36] of nematic director profiles in thin nematic films indicate that the value of K_{13} is small compared to other elastic constants.

An exact determination of elastic and surface properties of a nematic liquid crystal requires a knowledge of the stability regions of different structures and the dependence of structural details on elastic constants and the surface anchoring condition. However, most of the recent stability studies were restricted to an approximation of equal Frank nematic elastic constants in the absence of an external field. The surface elastic constants K_{24} and K_{13} were determined with a large uncertainty.

For this reason we decided to carry out a stability study of nematic structures in cylindrical cavities showing a dependence on elastic properties, homeotropic anchoring strength, and transversal external field. Emphasis is given to the dependence of stability regions on K_{24}. The paper is organized as follows. In Sec. II the model free energy and corresponding Euler-Lagrange equations are presented. In Sec. III the dependence of structures on model parameters is analyzed. In Secs. IV and V stability diagrams are presented in the absence and presence of an external field, respectively. In the last section we summarize results. A preliminary account of these results, where we focus on the similarity between nematic structures in a cylindrical capillary and spherical droplet, has already been presented [32].

II. MODEL

In order to study nematic structures confined to a supramicrometer cylindrical capillary we use the Frank [37,38] phenomenological approach. The length L of the capillary is assumed to be much larger than its radius R. Thus finite length L effects on a nematic structure can be neglected. We restrict our study to cavities with a supramicrometer radius deep in the nematic phase. This enables us to neglect spatial variations of the nematic orientational order parameter. Nematic structures are in this case well described by the director field $\mathbf{n}(\mathbf{r})$ alone [14]. The cavity wall is set to enforce the homeotropic anchoring.

The corresponding free energy density [24,37–39] in the nematic director field is

$$\begin{aligned} f(\mathbf{r}) = & \frac{K_{11}}{2}(\mathrm{div}\mathbf{n})^2 + \frac{K_{22}}{2}(\mathbf{n}\cdot\mathrm{curl}\mathbf{n})^2 + \frac{K_{33}}{2}(\mathbf{n}\times\mathrm{curl}\mathbf{n})^2 \\ & - \frac{K_{24}}{2}(\mathbf{n}\times\mathrm{curl}\mathbf{n} + \mathbf{n}\,\mathrm{div}\mathbf{n})\cdot\boldsymbol{\nu}\delta(\mathbf{r}-\mathbf{R}) \\ & + K_{13}(\mathbf{n}\,\mathrm{div}\mathbf{n})\cdot\boldsymbol{\nu}\delta(\mathbf{r}-\mathbf{R}) \\ & + \frac{W_0}{2}[1-(\mathbf{n}\cdot\boldsymbol{\nu})^2]\delta(\mathbf{r}-\mathbf{R}) - \frac{\Delta}{2}(\mathbf{n}\cdot\boldsymbol{\zeta})^2 . \end{aligned} \tag{1}$$

The nematic elastic properties are described in the splay (K_{11}), twist (K_{22}), bend (K_{33}), splay-bend (K_{13}), and saddle-splay (K_{24}) elastic constant. Note that different definitions of K_{24} are in use. We adopt the definition [1] $-K_{24}/2(\mathbf{n}\times\mathrm{curl}\mathbf{n}+\mathbf{n}\,\mathrm{div}\mathbf{n})$ used in recent publications of Allender and co-workers. Other forms are $-K_{24}(\mathbf{n}\times\mathrm{curl}\mathbf{n}+\mathbf{n}\,\mathrm{div}\mathbf{n})$ (e.g., Ref. [36]) and

$-(K_{24}+K_{22})(\mathbf{n}\times\text{curln}\times\mathbf{n}\,\text{divn})$ (e.g., Ref. [40]). The term with the constant W_0 [39] models the homeotropic anchoring imposed by the lateral wall of the cylinder. A short range character of the surface interaction is modeled with the δ function $\delta(\mathbf{r})$. The wall is located at $\mathbf{r}=\mathbf{R}$ and $\boldsymbol{\nu}$ is its normal. The last term in Eq. (1) describes the presence of an external magnetic or electric field $\boldsymbol{\zeta}=\zeta\mathbf{e}_f$ of magnitude ζ, pointing along the unit vector $\mathbf{e}_f$. The quantity Δ measures the magnetic or electric anisotropy of the liquid crystal. In this study we assume $\Delta>0$. As a consequence the external field tends to orient $\mathbf{n}$ along $\mathbf{e}_f$.

Recently a lot of attention has been devoted to the "surface" or, better, the recently designated [34] "divergence" elastic K_{13} and K_{24} terms. These two terms can be converted to surface integrals by the use of Gauss's theorem. Therefore, although the elastic constants K_{13} and K_{24} represent a fraction of the bulk free energy density they influence nematic structures only via boundary conditions. In contrast to Frank elastic constants, which are in leading order proportional to S^2, the leading term of surface elastic constants is proportional to S [40,41]. This is demonstrated in Appendix A. The K_{24} problem is mathematically well posed. Theoretical [42] and recent experimental studies [1,11] indicate that values of K_{24} and Frank elastic constants are comparable. However, much more ambiguity is related to the K_{13} contribution. Its peculiarity is that it introduces [34] derivatives along the surface normal direction. As a consequence, the functional (1) is not bounded from below. There are different suggestions on how to avoid this problem [33–36,43]. Recent estimations [33,35,36] based on different approaches suggest that K_{13} is smaller than the Frank elastic constants. For the K_{13} term as defined in Eq. (1), they yield $K_{13}\approx-0.2K_{11}$ [36], $-K_{13}<K_{11}/2$ and $-K_{13}<K_{33}/2$ [33], and $|K_{13}|\approx10^{-12}N$ [35]. But although K_{13} seems to be smaller than the remaining elastic constants it can play an important role [34]. The K_{13} term can be negative (in contrast to Frank elastic terms) and can cause spontaneous deformations. In this study we disregard the K_{13} contribution. We will return to this problem in a future work.

It is convenient to express anchoring and external field strength with corresponding typical lengths [24] $d=K_{11}/W_0$ and $\xi=\sqrt{K_{11}/(\zeta^2\Delta)}$, respectively. The surface coherence length d measures the competition between the nematic elastic and anchoring forces. The anchoring influence on a director profile becomes significant for $R/d>1$. The field correlation length ξ measures the competition between elastic forces and the external field. The field influence becomes important if $R/\xi>1$.

In calculations we use dimensionless cylindrical coordinates $\mathbf{x}$ in units of the cylinder radius R. Unit vectors along dimensionless coordinates ρ, φ, z are denoted with $\mathbf{e}_\rho$, $\mathbf{e}_\varphi$, $\mathbf{e}_z$, respectively. We introduce dimensionless operators $\nabla\cdot=R$ div, $\nabla\times=R$ curl, and ratios $\mu=R/d$, $a_i=K_i/K_{11}$, $i=\{22,33,24\}$.

Taking this into account the dimensionless free energy density $g(\mathbf{x})=f(\mathbf{r})/(K_{11}/R^2)$ is expressed as

$$g(\mathbf{x})=\tfrac{1}{2}[(\nabla\cdot\mathbf{n})^2+a_{22}(\mathbf{n}\cdot\nabla\times\mathbf{n})^2+a_{33}(\mathbf{n}\times\nabla\times\mathbf{n})^2]$$
$$-\frac{a_{24}}{2}(\mathbf{n}\times\nabla\times\mathbf{n}+\mathbf{n}\nabla\cdot\mathbf{n})\cdot\mathbf{e}_\rho\delta(\rho-1)$$
$$+\frac{\mu}{2}[1-(\mathbf{n}\cdot\mathbf{e}_\rho)^2]\delta(\rho-1)-\frac{R^2}{2\xi^2}(\mathbf{n}\cdot\mathbf{e}_f)^2\ . \tag{2}$$

In this study the external field is restricted to the $(\mathbf{e}_\rho,\mathbf{e}_\varphi)$ plane and points along $\mathbf{e}_f=\mathbf{e}_\rho\cos\varphi-\mathbf{e}_\varphi\sin\varphi$.

The minimization of the corresponding dimensionless free energy $G=\int g(\mathbf{x})d^3\mathbf{x}$ yields the Euler-Lagrange differential equations. We study only structures without the twist deformation. This step is in accordance with experimental studies [1] in long cylinders subject to homeotropic anchoring, which do not reveal structures with pronounced twist deformation.

We use different parametrization for the escaped radial and polar structures. In the case of a negligible external field strength ($R/\xi<1$) the director field of ER structures can be solely described by the angle $\theta(\rho,z)$: $\mathbf{n}=-\mathbf{e}_\rho\sin\theta+\mathbf{e}_z\cos\theta$. The corresponding bulk equilibrium equation is (discarding the external field term)

$$\rho^2\frac{\partial^2\theta}{\partial z^2}(a_{33}\cos^2\theta+\sin^2\theta)+\left[\rho^2\frac{\partial^2\theta}{\partial\rho^2}+\rho\frac{\partial\theta}{\partial\rho}\right](\cos^2\theta+a_{33}\sin^2\theta)-\sin\theta\cos\theta$$
$$+\frac{(a_{33}-1)}{2}\left\{\sin(2\theta)\left[\rho^2\left[\frac{\partial\theta}{\partial\rho}\right]^2-\rho^2\left[\frac{\partial\theta}{\partial z}\right]^2-\rho\frac{\partial\theta}{\partial_z}\right]-2\rho^2\left[\sin(2\theta)\frac{\partial^2\theta}{\partial\rho\partial z}+\cos(2\theta)\frac{\partial\theta}{\partial\rho}\frac{\partial\theta}{\partial z}\right]\right\}=0\ . \tag{3a}$$

The boundary condition at $\rho=1$ is given by

$$\frac{\partial\theta}{\partial\rho}(\cos^2\theta+a_{33}\sin^2\theta)+\frac{\partial\theta}{\partial z}\sin\theta\cos\theta(1-a_{33})$$
$$+(1-\mu-a_{24})\sin\theta\cos\theta=0\ . \tag{3b}$$

Note that for the escaped radial structures the K_{24} term simply renormalizes the anchoring μ (see Appendix B). Thus the saddle-splay contribution for such cylindrical symmetry does not introduce a qualitatively new "anchoring" source at the cylinder wall. It is to be stressed that conventionally the K_{24} term enters the boundary condition together with director derivatives [34]. The detailed derivation of Eq. (3b) is given in Appendix B.

The remaining boundary conditions are $\theta(\rho=0)=0$; the ERPD director field is enforced by

$\theta(\rho,z=0)=\theta(\rho,z=1=l_{PD})=\pi/2$ and the ER director field does not depend on the z coordinate. Here $z=0$ and $z=l_{PD}=L_{PD}/R$ describe the position of two adjacent planes with a planar radial director configuration of the ERPD structure.

The polar structures are described by the angle $\phi(\rho,\varphi)$, where $\mathbf{n}=\mathbf{e}_\rho\cos\phi+\mathbf{e}_\varphi\sin\phi$. The corresponding bulk differential equation reads

$$(1-a_{33})\left\{\sin(2\phi)\left[\left[\frac{\partial\phi}{\partial\rho}\right]^2\rho^2-\left[\frac{\partial\phi}{\partial\varphi}\right]^2+1-2\frac{\partial^2\phi}{\partial\rho\partial\varphi}\rho\right]-2\cos2\phi\frac{\partial\phi}{\partial\rho}\frac{\partial\phi}{\partial y}\rho\right\}$$
$$+2\left[\frac{\partial^2\phi}{\partial\rho^2}\rho^2+\frac{\partial\phi}{\partial\rho}\rho\right](\sin^2\phi+a_{33}\cos^2\phi)+2\frac{\partial^2\phi}{\partial\varphi^2}(a_{33}\sin^2\phi+\cos^2\phi)-\left[\frac{R}{\xi}\right]^2\rho^2\sin[2(\phi+\varphi)]=0\ , \quad (3c)$$

with the boundary condition at $\rho=1$:

$$\frac{\partial\phi}{\partial\rho}(a_{33}\cos^2\phi+\sin^2\phi)$$
$$+\sin\phi\cos\phi\left[(a_{33}-1)\left[\frac{\partial\phi}{\partial\varphi}+1\right]+\mu\right]=0\ . \quad (3d)$$

In planar structures the K_{24} contribution is absent [1] and therefore does not enter Eq. (3d). The equations are solved numerically for different ratios of elastic constants, values of the anchoring, and the external field strength using the relaxation method [44].

The stability diagrams are obtained by comparing free energies of different structures. To avoid singularities in free energy density at defect sites the isotropic core surrounding the defect is introduced [2]. The core radius is approximately given by a nematic coherence length. We test the adequacy of this approach in the case of the PR structure. For this simple structure we evaluate the corresponding free energy deep in the nematic phase taking into account $S(\mathbf{r})$ variation (Appendix C). Comparison with a free energy value obtained via the approximation of a constant order parameter shows a negligible discrepancy (far below 1%, which is the accuracy of our calculations).

III. STRUCTURES

Recent experimental studies [1] indicate that among structures for the geometry and surface conditions described the ER and PP structures are most often realized. For this reason we first analyze the dependence of these structures on elastic properties and anchoring strength.

A. Escaped radial structure

The escaped radial structure for different ratios a_{33} and anchoring strengths has already been studied by Allender and co-workers [1]. They have derived the analytic expression for the ER director field in the absence of an external field. They have shown that its structure can be presented alone by the surface parameter $\sigma=a_{24}+\mu-1$ and the ratio a_{33}. In the following we present the main features of the ER structure in order to understand stability diagrams that we intend to calculate.

The angle $\theta(\rho)$, the average orientational parameter $\langle P_2\rangle$ (see details in the last lines of this section), and $\theta(\rho=1)$ dependence on σ and a_{33} are plotted in Figs. 2 and 3, respectively. For large cylinder radia ($R/d\gg1$) the value of σ is dominated by a relative anchoring strength $\mu=R/d$. With decreased radius the a_{24} contribution in σ becomes important. Figures 3(a) and 3(b) reveal that the ER structure is (meta)stable only if $\sigma\geq1$ for any a_{33} ratio. Below $\sigma=1$ the ER director field continuously transforms into the homogeneous structure. In this configuration the director field is homogeneous, oriented parallel to the $\mathbf{e}_z$ direction [$\theta(\rho)=0$]. Above the threshold $\sigma=1$, with increased σ, the ER structure continuously develops. For $\sigma\gg1$ the surface angle $\theta(\rho=1)$ asymptotically approaches its strong anchoring limit $\pi/2$.

The ER director field qualitative response to the a_{33} variation depends on the anchoring regime. If σ is small enough (the weak anchoring regime), the director structure mostly adapts to an a_{33} variation by changing

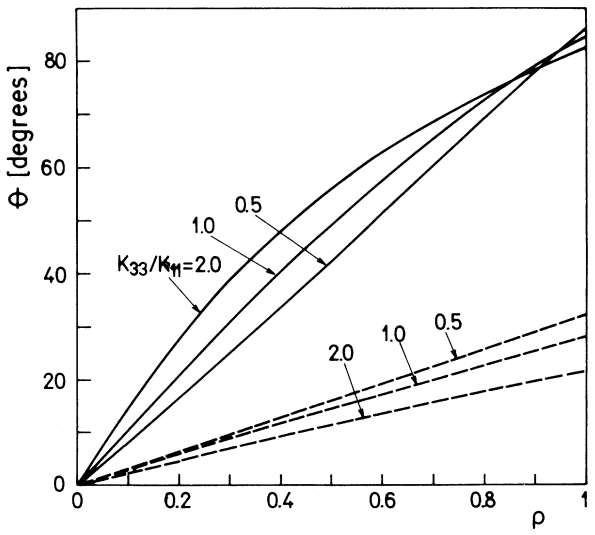

FIG. 2. ER director field as a function of ρ for different ratios of elastic constants. Dotted line: $\mu+K_{24}/K_{11}=2.1$; full line: $\mu+K_{24}/K_{11}=12$.

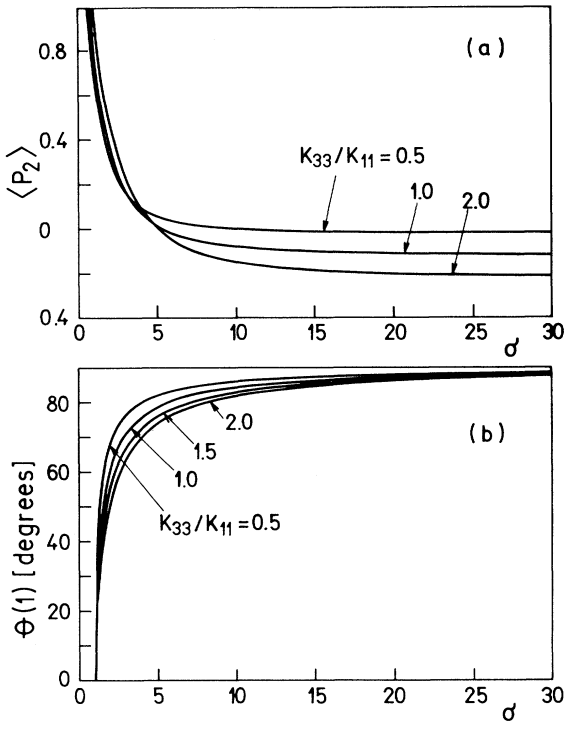

FIG. 3. ER structure dependence on $\sigma=\mu+K_{24}/K_{11}-1$ and K_{33}/K_{11} represented by (a) $\langle P_2 \rangle=\langle 3\mathbf{n}\cdot\mathbf{e}_z^2-1 \rangle/2$ and (b) director field orientation $\theta(\rho=1)$ at the wall of the cylinder.

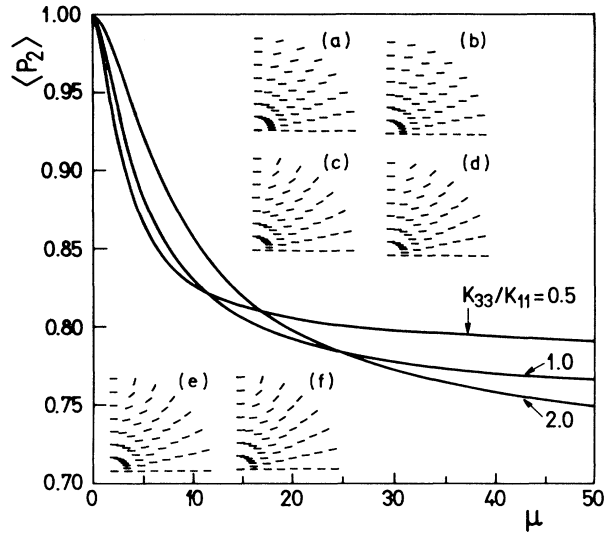

FIG. 4. Average director field variation of the PP structure, represented by $\langle P_2 \rangle=\langle 3\mathbf{n}\cdot\mathbf{N}_{PP}^2-1 \rangle/2$, with μ and $a_{33}=K_{33}/K_{11}$. The unit vector $\mathbf{N}_{PP}$ points along the average director field orientation. In the inset the director field of the PP structure for (a) $\mu=1$, $a_{33}=0.5$; (b) $\mu=1$, $a_{33}=2$; (c) $\mu=10$, $a_{33}=0.5$; (d) $\mu=10$, $a_{33}=2$; (e) $\mu=\infty$, $a_{33}=0.5$; (f) $\mu=\infty$, $a_{33}=2$ are shown.

$\theta(\rho=1)$, which is evident from Fig. 2. The qualitative course of $\theta(\rho)$ is preserved. Increased a_{33} decreases the $\theta(\rho=1)$ value and this reduces the average bend deformation. In the strong anchoring regime ($\sigma>20$) the surface anchoring interaction fixes $\theta(\rho=1)$ to $\pi/2$. In this case the ER structure reduces its deformational free energy by shifting the region of strongest bend deformation towards the center of the cylinder with increased a_{33}. In Fig. 3(a) the variation of the ER structure as a function of a_{33} and σ is represented via the average orientation parameter $\langle P_2 \rangle=\langle 3\mathbf{n}\cdot\mathbf{N}_{ER}^2 1 \rangle/2$ dependence. Here $\langle \ldots \rangle$ stands for the average over the cylinder volume and $\mathbf{N}_{ER}$ points along the average director field orientation; thus $\mathbf{N}_{ER}=\mathbf{e}_z$. This quantity can be, e.g., directly experimentally determined by the deuterium [1,30] or proton NMR in small cavities ($R<1$ μm), or indirectly by the optic polarization experiment [10,11] in large cavities ($R>1$ μm).

B. Planar polar structure

In the PP structure, schematically presented in Fig. 1(d), the strongest elastic deformations are localized near diametrically lying points at the cylinder surface. With increased anchoring strength these regions tend to develop into line defects of strength [23] $\frac{1}{2}$ in order to reduce the surface free energy contribution. This is evident from the inset of Fig. 4. The PP director field does not depend on a_{24}. Namely, for planar structures [1] $\mathrm{div}(\mathbf{n}\cdot\mathrm{div}\mathbf{n}+\mathbf{n}\times\mathrm{curl}\mathbf{n})=0$. Therefore in the absence of an external field its structure is determined by a_{33} and μ values alone.

Dependence of $\langle P_2 \rangle$ of the PP structure on a_{33} and μ is shown in Fig. 4. In the weak anchoring regime increased a_{33} reduces average departures of the director field from the homogeneous structure. As a consequence $\langle P_2 \rangle$ is increased with a_{33} for $\mu<10$. This reduces the bulk elastic free energy at the expense of the cheap surface anchoring penalty. If the anchoring strength is considerable ($\mu>15$) the surface anchoring does not allow significant deviation of the surface nematic director field from the normal (easy) direction. The major structural changes with the increased a_{33} ratio are therefore realized in the cylinder interior.

C. Free energy dependence on elastic and anchoring properties

The resulting free energies F_s of structures [$s=$(PP,ER)] are plotted in Fig. 5 as a function of $\mu=R/d$ for different ratios of elastic constants. As already discussed, the free energy F_{PP} at the PP structure does not depend on a_{24}. A large positive value of a_{24} stabilizes the ER structure with respect to the PP director field. For a given a_{24} value the $F_{ER}=F_{ER}(\mu)$ dependence is plotted above $\mu=\mu_{ER}=2-a_{24}$, corresponding to $\sigma=1$. Below μ_{ER} the ER structure transforms into the homogeneous structure (Sec. III A). Above $\mu\sim10$ the ER free energy only slightly changes (for typical a_{33} values), with μ indicating that the strong anchoring condition is already well established. The free energies of the PP and

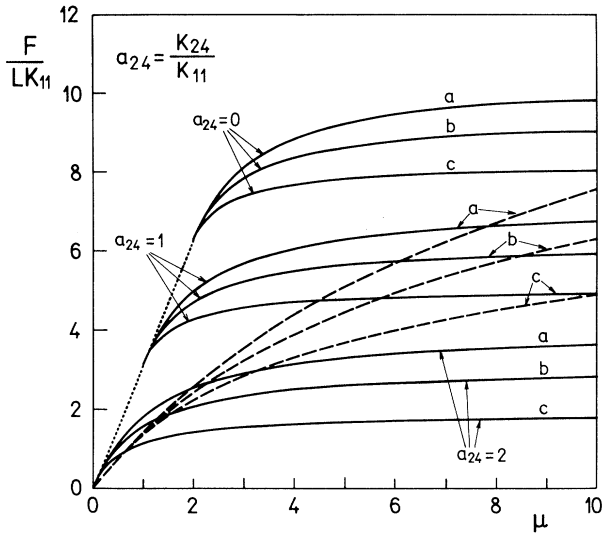

FIG. 5. Free energy dependence of the PP (dashed line), ER (full line), and homogeneous structure (dotted line) on μ, $a_{33}=K_{33}/K_{11}$, and $a_{24}=K_{24}/K_{11}$. Lines denoted with letters (a), (b), (c) correspond to the cases $a_{33}=1.5$, $a_{33}=1$, and $a_{33}=0.5$, respectively.

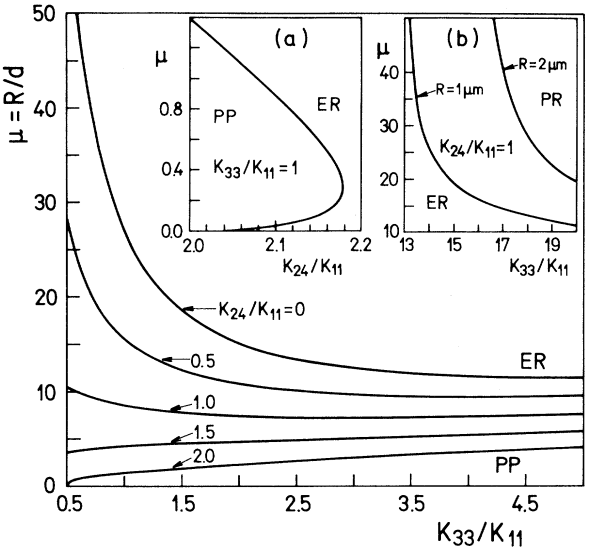

FIG. 6. Stability diagram of the ER and PP structures in the $(\mu=R/d, K_{33}/K_{11})$ plane in the absence of an external field. In the inset (a) the stability diagram as a function of μ and K_{24}/K_{11} is shown for $K_{33}/K_{11}=1$ and $K_{24}/K_{11}\geq 2$. The regime of very large K_{33}/K_{11} values, where the PR structure can be stable, is demonstrated in the inset (b) for $K_{24}/K_{11}=1$.

ER structure are strongly a_{33} dependent because both configurations contain a considerable amount of bend deformation.

IV. STABILITY DIAGRAM IN THE ABSENCE OF AN EXTERNAL FIELD

In the stability study we consider only the case $K_{24}>0$. Theoretically [42] $K_{24}<0$ is also allowed. But to our knowledge all recent experiments suggest that K_{24} is positive [1,11]. In the weak anchoring regime negative K_{24} could cause $\sigma<0$. But this regime is rather "boring" since already below $\sigma=1$ the ER structure is replaced by a homogeneous one.

The stability diagram of the PP and ER structure in the (μ,a_{33}) plane in the absence of an external field for different a_{24} values is presented in Fig. 6. The stability regions of the structures are separated by the coexistence line $\mu_0=\mu_0(a_{33})$. The topology of the ER structure allows a perfect match of the homeotropic boundary condition for large μ values. Therefore for the chosen values of material parameters the ER structure is stable for $\mu\geq\mu_0$ and the PP structure for $\mu\leq\mu_0$.

Qualitative characteristics of the stability diagram depend on the a_{24} value.

(i) If $a_{24}<1$ the transition between the two competing structures occurs in the regime where the anchoring strength is considerable ($\mu>10$). The a_{33} ratio has a relatively weak influence on the director field at the cylinder surface. Therefore the bend contribution to the deformation free energy in the PP structure is larger than in the ER one. As a consequence, with increased a_{33} a coexistence relative anchoring strength μ_0 is decreased. But for $a_{33}\gg 1$ the K_{33} influence is strong enough to change the director orientation at the cylinder surface, particularly that of the PP structure. This reduces the bend contribution of the free energy of PP more than that of the ER structure. As a consequence, μ_0 is slightly increased with increased a_{33}.

(ii) If $a_{24}>1$ the transition takes place for all a_{33} values in the weak anchoring regime. Enabling apparent changes of the director field at the cylinder wall causes μ_0 to increase with increased a_{33} as already discussed above. If a_{33} is small enough and $a_{24}>1.5$ the ER structure can even be stable for all μ values.

(iii) For $a_{24}>2$ the stability diagram is qualitatively different. Since these values of a_{24} are most probably not realized, only the case of $a_{33}=1$ is studied. The corresponding stability diagram is presented in the inset (a) of Fig. 6. We see that an additional stability region of the ER structure appears, extending from $\mu=0$ to μ_0', designating the lower lying $\mu_0=\mu_0(a_{33})$ branch. This is due to the existence of the ER structure until $\mu=0$ for $a_{24}>2$. At $\mu=0$ the condition $F_{PP}=0>F_{ER}$ is true because of the strong a_{24} contribution in F_{ER}. With increased relative anchoring strength μ the ER structure experiences more pronounced changes than the PP director field. As a consequence the PP structure becomes stable at $\mu=\mu_0'$. At still higher μ values the ER structure is reentered at μ_0 due to the smaller surface free energy contribution. For $a_{24}>a_{24}^c$ [$a_{24}^c(a_{33}=1)\approx 2.18$] the μ_0 and μ_0' branches meet, resulting in the stability of the ER structure for all anchoring strengths.

Near the nematic–smectic-A transition the bend elastic constant K_{33} is anomalously increased due to the pre-

transitional effects [23]. In this case the PR structure can be stabilized because its director field has only splay deformation. This is demonstrated in the inset (b) of Fig. 6. Because of the presence of the line defect in the PR structure, the stability diagram no longer depends on R only via the ratio R/d. With increased R a stability region of the PR structure is reduced. This happens because the core size surrounding the defects and its contribution to the free energy are almost independent [2] of R. With increased R a relative fraction of the defect-core region is reduced. A relative volume with strongly established nematic order is enhanced, increasing the elastic free energy contribution.

The stability diagram shown in Fig. 6 suggests how the ER-PP transition can be used for the K_{24} determination. Particularly convenient is the $a_{33}>1$ regime assuming $a_{24}\in[0,2]$. Coexistence lines $\mu_0=\mu_0(a_{33})$ lie in the regime, where (i) both structures studied strongly depend on μ_0 and (ii) the coexistence relative anchoring strength μ_0 weakly depends on a_{33}. The amount of structural changes is clearly visible from $\langle P_2\rangle=\langle 3\mathbf{n}\cdot\mathbf{N}_s^2-1\rangle/2$ dependence, shown in Figs. 3(a) and 4. Here $\mathbf{N}_s$ stands for the average director field of the planar polar ($s=$PP) and escaped radial structure ($s=$ER). A $\langle P_2\rangle$ value of the ER and PP structure at the coexistence point can reveal a_{24} and μ values. A possible way of extracting K_{24} from $\langle P_2\rangle$ data is presented in detail in Refs. [2,45]. Since for $a_{33}>1$ the coexistence relative anchoring strength μ_0 only weakly depends on a_{33}, the most convenient way of finding μ_0 is by changing the cylinder radius or weakening the anchoring strength at constant temperature. This has already been done by Allender and co-workers [1] using the deuterium NMR experiment in which they estimated a K_{24} value for the first time. It should be mentioned that details of the ER structure in its range of stability also reveal relatively well a K_{24} magnitude if ratios a_{33} and μ are known. Polak *et al.* [11] took advantage of this fact and obtained estimations of K_{24} in supramicrometer cylinders using an optic polarization experiment.

V. STABILITY DIAGRAM IN THE PRESENCE OF AN EXTERNAL FIELD

In the following the external field $\boldsymbol{\zeta}=\zeta\mathbf{e}_f$ is introduced in the $(\mathbf{e}_\rho,\mathbf{e}_\varphi)$ plane. The external field forces the average director field of the PP structure to point along $\mathbf{e}_f$. In calculations only the external field induced distortions of the PP structure are taken into account. To study this effect in the ER structure another angle in addition to $\theta(\rho)$ has to be introduced to describe $\mathbf{n}$ because of the broken cylindrical symmetry. To avoid this technical complication we estimate $\mathbf{n}$ distortions in the planar PR structure. This structure is topologically equivalent to the ER structure. The analyses show that the free energy changes ($\sim 1\%$ deviation) due to the PR director field distortions induced by ζ are negligible in the regime, where ER structure is stable. Note that in this regime the PR director field in general apparently deviates from "pure" radial distribution. But the reduction of the external field free energy contribution is accompanied by a comparable increase in the elastic free energy component. This suggests that the approximation used is reasonable, at least in the regime of stronger anchoring ($\mu>10$).

A. Weak anchoring regime

The resulting stability diagram in the weak anchoring regime dependent on the elastic properties, external field, and anchoring strength is shown in Fig. 7. The stability regions of the ER and PP structure are separated by the

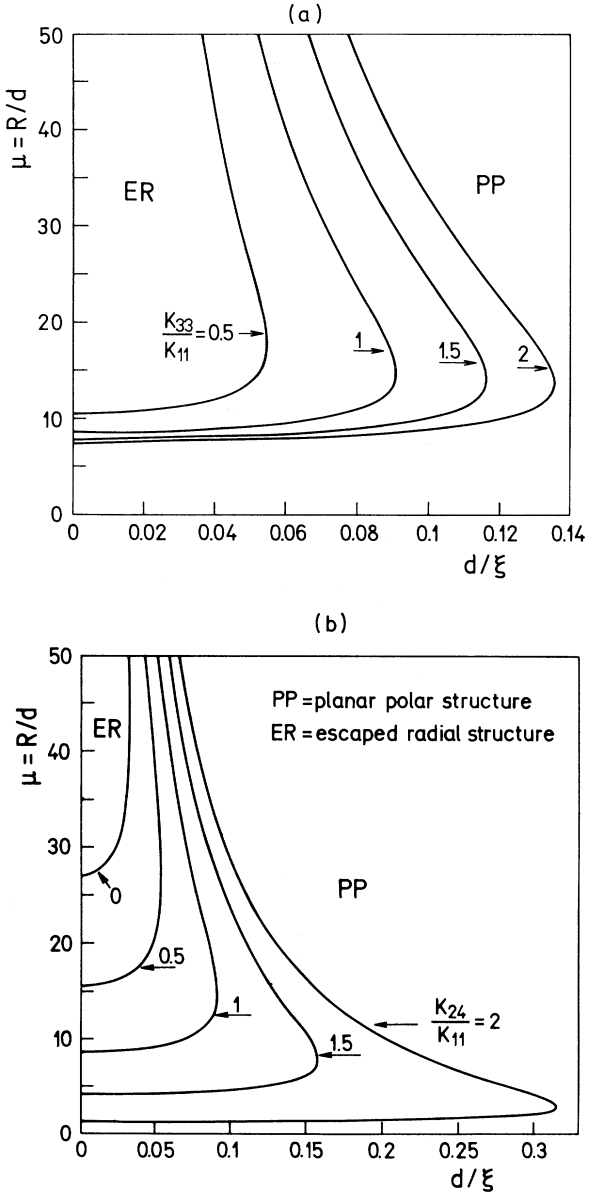

FIG. 7. Stability diagram of the PP and ER structures as a function of dimensionless quantities $\mu=R/d$ and d/ξ for (a) different ratios of K_{33}/K_{11}; $K_{24}/K_{11}=1$; (b) different ratios of K_{24}/K_{11}; $K_{33}/K_{11}=1$.

coexistence line $(d/\xi)_c=(d/\xi)_c(\mu)$. The escaped radial structure is stable in the $d/\xi<(d/\xi)_c$ region. Since the average director field of the planar polar structure is closer to the external field direction than that of the ER structure, the increased external field strength prefers the PP director pattern. The stability diagram is qualitatively the same for all a_{33} values assuming $a_{24}<2$. With increased a_{33} the ER domain is increased because the ER structure has in almost all cases (see Sec. IV) relatively less of a bend contribution compared to the PP director field. The $(d/\xi)_c$ line has two characteristic points: the inversion point $\{(d/\xi)_i,\mu_i\}$, where the line $(d/\xi)_c$ reaches maximum, and the zero field coexistence point $\{0,\mu_0\}$, where $(d/\xi)_c$ equals zero.

B. Strong anchoring regime

1. Stability of planar structures with respect to the ER structure

With increased anchoring strength the areas of highly deformed PP structure tend to develop into two surface line defects of strength $S_d=1$ [46]. Let us call the resulting structure the planar polar structure with surface line defects (PPSLD's). The topology of the problem allows us to push these line defects away from the surface toward the center of the cylinder. Consequently the strength of both defects is reduced [46] to $S_d=\frac{1}{2}$. We name this structure the planar polar structure with line defects. In the limiting case the two line defects meet at the cylinder axis merging into a single defect of strength $S_d=1$, forming the planar radial structure. In turn the $S_d=1$ defect of the PR structure can continuously escape along the cylinder axis, forming the ER structure with a nonsingular core. Therefore the PPSLD, PPLD, PR, and ER structures are topologically equivalent [20] and can be continuously transformed into each other by changing relevant parameters.

Before taking into account all of these structures in our stability study we first briefly analyze the influence of the defect strength S_d on the distortion free energy. Investigations of defects in a thin nematic film [23] show that a defect contribution to the elastic free energy is proportional to S_d^2. If a defect is moved to the surface it occupies only half of its volume in the bulk, but its strength is doubled. The latter assumption is valid in the strong anchoring case. In this respect the PPLD with two defects of strength $S_d=\frac{1}{2}$ is energetically advantageous with respect to the PR and PPSLD director field. But these are only rough estimations neglecting a finite anchoring and external field effects.

The numerically obtained stability diagram, taking into account the ER, PR, PP, PPLD, and PPSLD director fields, is shown in Fig. 8. We see that among structures with line defects only the PPLD structure can be stable in the regime of chosen elastic properties. The PPLD director field has a lower surface free energy contribution than the PP structure and a lower external field contribution than the ER structure. This property makes it stable in an interval of the external field strength in the strong anchoring regime. The coexistence lines between ER-PPLD and PPLD-PP structures meet at the triple point $((d/\xi)_{tp},\mu_{tp})$. At the ER-PPLD coexistence line the R/ξ ratio is constant. This is the consequence of the dependence of ER and PPLD structures only on R/ξ in the strong anchoring regime for a fixed set of nematic elastic constants [see Eqs. (3)].

The existence of the PPLD structure breaks the scaling property of the $(d/\xi,\mu)$ stability diagram. The presence of line defects, as already discussed in the case of the PR structure, introduces a dependence on the cylinder radius.

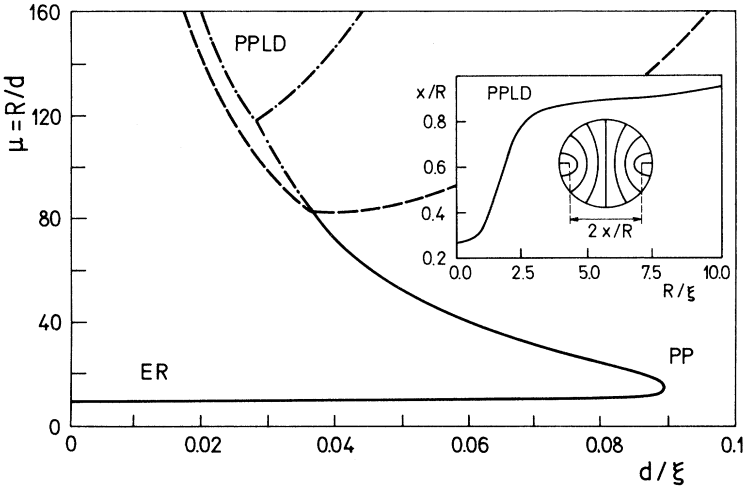

FIG. 8. Stability diagram of the planar polar (PP), planar polar structure with two line defects (PPLD), and escaped radial structure (ER) as functions of dimensionless quantities $\mu=R/d$ and d/ξ for $R=1$ μm (full and dashed lines) and $R=2$ μm (full and dash-dotted lines). In the inset the dependence of the line-defects separation of the PPLD structures on the external field strength is shown.

The relative separation x of line defects in the PPLD structure depends on the external field strength, which is demonstrated in the inset of Fig. 8. Note that only in a part of the plot shown is the PPLD director stable. For $d/\xi=0$ and $a_{33}=1$ the line-defect separation is $2x\sim 0.6R$. The anomalous increase in x with increased external field strength indicates that at $R/\xi\sim 2$ the external field influence on x becomes prevailing.

2. *Stability of planar structures with respect to the ERPD structure*

Until now we have compared the planar structures with the defectless ER director pattern. In practice such a structure can be realized only in long and large cylinders ($R\gg 1\mu$m, $L/R\gg 1$) where the roughness of the surface and effects of the cylinder ends have a negligible influence on **n**. In other cases point defects are usually incorporated into the ER director field. In long narrow cylinders a metastable ERPD structure is observed [29,30]. The average distance $L_{\rm PD}$ among point defects of cylinders of $R\approx 0.2-0.3$ μm is estimated [30] to be between $2R$ and $3R$. A section of this structure between two adjacent planar planes can even be stable in a cylinder of finite length L in which the lateral wall enforces homeotropic, and the other two limiting surfaces strong isotropic, tangential anchoring. Reminiscent structures have been studied by Liang and Chen [7].

In the following we study a stability diagram where the ER structure is replaced by the ERPD one (or equivalently by the ERPD section in a finite cylinder). We limit our study to the cases of $L_{\rm PD}/R=2$ and $L_{\rm PD}/R=3$. The resulting stability diagram is presented in Fig. 9. The cases of ER and ERPD with $L_{\rm PD}/R=2$ and $L_{\rm PD}/R=3$ are superimposed for $a_{24}=1$. The replacement of the ER structure does not affect qualitative features of the stability diagram. The main quantitative changes are the following.

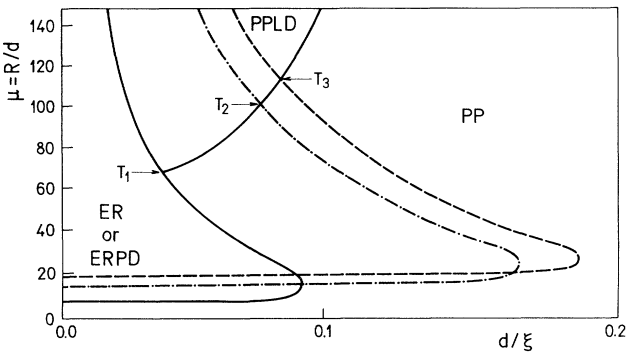

FIG. 9. Stability diagram of the planar polar structure (PP), planar polar structure with two line defects (PPLD), escaped radial (ER) structure, and escaped radial structure with point defects (ERPD) for $L_{\rm PD}/R=2$ and $L_{\rm PD}/R=3$ as functions of dimensionless quantities $\mu=R/d$ and d/ξ. The full line separate the stability regions of ER, PP, and PPLD structures. The dash-dotted and full line right from the triple point T_2 separates the regions of the PP, PPLD, and ERPD structure with $L_{\rm PD}/R=3$. The dashed and full lines right from the triple point T_3 separate the regions of the PP, PPLD, and ERPD structure with $L_{\rm PD}/R=2$.

(i) Since the ERPD structure is more energetic than the ER one, the zero field coexistence point μ_0 is shifted toward higher values. The coexistence line $(d/\xi)_c$ is also pushed toward higher values. This is due to planar radial domain walls in the ERPD structure that have a lower external field free energy contribution with respect to the uniformly escaped structure.

(ii) The ERPD structure with larger $L_{\rm PD}$ has lower μ_0 because $F_{\rm ERPD}$ with increased $L_{\rm PD}$ decreases [29]. This is true in the repelling regime of point defects, where $L_{\rm PD}$ is larger than the critical separation $L_{\rm PD}^{(c)}$. With increasing $L_{\rm PD}$ the ratio $(d/\xi)_c$ decreases because a relative number of planes with the planar radial structure is reduced.

3. *Existence of the PPLD structure in the absence of an external field*

In thermotropic uniaxial nematics the PPLD structure has not yet been observed. But a reminiscent structure has been recently observed in a biaxial micellar nematic liquid crystal using optical polarization microscopy by Liu and Saupe [47]. They investigated textures and defects in capillaries of micellar nematics. They show that biaxial micellar nematics have two line defects of strength $\frac{1}{2}$ running parallel to the capillary axis in a helical fashion. This structure is stable in the absence of an external field. The distance between line defects is estimated to be $\frac{2}{3}$ of the capillary diameter.

Guided by this experiment we also have tried to stabilize the PPLD structure of our uniaxial model in the absence of an external field ζ. For this reason we replaced the ER structure with the more energetic ERPD one. But for reasonable values of parameters the qualitative features of the ER-PPLD-PP stability diagram are preserved. Actually, we find that the PPLD structure could be stabilized at $\zeta=0$ for relatively low values of a_{24}, R, and the separation $L_{\rm PD}$ between line defects. We achieved this, e.g., for a set of values $a_{24}=0$, $L_{\rm PD}=2R$, $R=1$ μm. There are also other combinations, but for a reasonable choice of R and $L_{\rm PD}$ it is necessary that $a_{24}\approx 0$. This contradicts recent experimental estimations, which suggest [1,11] $a_{24}>1$.

We therefore suspect that the biaxiality is important for the stability of the PPLD-like structure observed by Liu and Saupe. We expected that among different effects related to biaxiality the K_{24} term is crucial. The free energy of the uniaxial PPLD structure is namely not affected by the saddle-splay elastic constant; the K_{24} contribution of the cylinder wall is canceled by the K_{24} contribution of the nematic-isotropic interface surrounding the line defects. Our intuitive expectation was that replacing the isotropic core with a biaxial one would have removed the canceling effect. That would cause a similar K_{24} dependence of the PPLD and radial-like structures. As a consequence the PPLD director structure could be stabilized for $\zeta=0$ for an optional K_{24} value. But in Ap-

pendix D we show that also in the biaxial case in planar structures the K_{24} contribution is irrelevant. Thus the twist character of the experimentally observed structure is presumably the relevant stabilizing parameter.

C. Hysteresis

In stability diagrams shown (Figs. 6–9) the stability regions of structures are separated by coexistence lines for which the condition $F_{S_1}=F_{S_2}$ applies. Here S_1, S_2 symbolize the competing structures and F_S is the corresponding free energy. However, most of the transitions studied are discontinuous and the states S_1 and S_2 are separated by an energy barrier ΔF. The system can surmount ΔF in a fluctuating manner. Thus the condition for the actual transitions $S_1 \rightarrow S_2$ is in general more demanding [6]; it requires $F_{S_1} \geq F_{S_2}$ and in addition $\Delta F \leq \Delta F_{\max}$. Here $\Delta F_{\max}$ describes the maximal energy barrier height, which can be overcome by fluctuations. Therefore an experimentally determined stability diagram could substantially differ from those shown in this work.

In order to estimate this we roughly estimate (i) the energy barrier ΔF between the ER and PP structures and (ii) the shift of the critical external field due to hysteresis phenomena in the case when the external field is continuously increased from zero.

To estimate the upper bound of ΔF we replace a discontinuous direct transition ER$\rightarrow$PP by a continuous evolution: ER$\rightarrow$PR$\rightarrow$PPLD$\rightarrow$PP. In this scenario the z component of the ER director field is continuously pushed toward zero until it transforms into the PR structure. The line defect of strength $S_d=1$ then splits into two line defects of $S_d=\frac{1}{2}$ which are pushed toward the cylinder wall. At the surface the discontinuity of $\mathbf{n}$ is relaxed if anchoring is not too strong. Let us assume that in this transformation the PR structure is most energetic (see the discussion in Sec. V B 1). Therefore the energy barrier of the transformation is $\Delta F \approx F_{\rm PR}-F_{\rm ER}$. In the absence of external field, equal elastic constants $K \equiv K_{11}=K_{33}$ and for $\mu \gg 1$ we get

$$\Delta F \approx \pi K L[\ln(R/\rho_c)-(3-a_{24})] . \tag{4}$$

Here ρ_c describes the core radius of the isotropic fluid surrounding the line defects of the PR structure (see Appendix C). For $R=1$ μm, $a_{24}=1$, and for a typical liquid crystal we get $\rho_c \approx 5$ nm, $\Delta F/(KL) \approx 10.4$. We see that the energy barrier logarithmically increases with R. Thus the hysteresis effects are more pronounced in large cylinders.

We now estimate the maximal shift of the $(R/\xi)_c$ value, where the ER$\rightarrow$PP transformation occurs, due to hysteresis effects. The ratio R/ξ is a convenient combination because for constant elastic properties and in the strong anchoring regime the director field depends only on R/ξ [see Eq. (2)].

In the approximation of equal elastic constants, assuming $\mu \gg 1$, we roughly express free energies of the ER, PP, and ER as [1]

$$F_{\rm ER} \approx \pi K L \left[3-a_{24}-\frac{(-1+2\ln 2)}{2}\left[\frac{R}{\xi}\right]^2 \right] , \tag{5a}$$

$$F_{\rm PR} \approx \pi K L \left[\ln\left[\frac{R}{\rho_c}\right]-\frac{1}{4}\left[\frac{R}{\xi}\right]^2 \right] , \tag{5b}$$

$$F_{\rm PP} \approx \pi K L \left[\ln\left[\frac{\mu}{4}\right]+1-\frac{1}{2}\left[\frac{R}{\xi}\right]^2 \right] . \tag{5c}$$

In this approximation the ER-PP coexistence value $(R/\xi)_c$ is defined by $F_{\rm ER}=F_{\rm PP}$, yielding $(R/\xi)_c \approx \sqrt{[\ln(\mu/4)-2+a_{24}]/0.3}$. For $\mu=50$, $a_{24}=1$, we get $(R/\xi_c \approx 2.3$, which is roughly in accordance with more detailed numerical calculation. We estimate the maximal shift of $(R/\xi)_c=(R/\xi)_{c,\max}$ with increased field by putting $F_{\rm ER} \approx F_{\rm PR}$, i.e., $\Delta F \approx 0$ and $F_{\rm PP} \ll F_{\rm ER}$. This is the latest stage when the ER structure overcomes the energy barrier before transforming into the PP structure. In this case even infinitesimally small fluctuations cause transformation into the PP director field. We get $(R/\xi)_{c,\max} \approx \sqrt{[\ln(R/\rho_c)-3+a_{24}]/0.5}$. For $R=1$ μm, $\rho_c=5$ nm, $a_{24}=1$, this estimation yields $(R/\xi)_{c,\max} \approx 8 \gg (R/x)_c$. Note that the latter approximation is very rough. In such high fields the PR structure is strongly deformed. It adopts a domainlike structure in which two halves of almost uniformly aligned $\mathbf{n}$ along the external field direction are separated by a strongly deformed band of thickness $\approx 2\xi$. In this structure the external field free energy contribution is minimized at the expense of strongly localized elastic distortions. Similar phenomena have been studied in detail in Ref. [6] in spherical droplets.

Our estimations suggest that hysteresis effects are important, particularly in large cylinders. Therefore in an experiment both directions of a critical parameter causing structural transition should be checked.

VI. CONCLUSIONS

We have numerically studied the stability of different nematic director structures in a long cylindrical capillary subjected to homeotropic anchoring. We use the Frank phenomenological approach in the representation of the uniaxial nematic director field. We construct stability diagrams of the ER, ERPD, PR, PP, and PPLD director fields dependent on (i) ratios of elastic constants K_{33}/K_{11}, K_{24}/K_{11}, (ii) the anchoring strength, and (iii) the transversal external field. The K_{13} contribution is discarded in this work. We show which sections of stability diagrams are most adequate for the experimental determination of the saddle-splay elastic constant. In addition, we demonstrate that in a finite interval of an external field strength in the strong anchoring regime the planar polar structure with two line defects can be stable. This structure has not been observed yet in thermotropic liquid crystals.

Note added. After finishing the paper we received the

article [48] in which Faetti proposes an alternative mathematical treatment of the K_{13} term consistent with Barbero-Oldano [43] K_{13} theory. According to his approach, K_{13} can in some cases apparently influence nematic structures confined to a cylindrical environment. In particular, it can induce surface structural transition. In a future paper we are going to study structures in a cylindrical cavity with emphasis on the K_{13} elastic constant and compare the consequences of contradicting Faetti's [48] and Pergamenshchik's [34] K_{13} approaches.

APPENDIX A: RELATIONS BETWEEN NEMATIC ELASTIC CONSTANTS

In this appendix we express the temperature dependent elastic constants K_i ($i \in [11,22,33,24,13]$) with temperature independent Landau expansion coefficients $L_i^{(j)}$ (i and j are positive integers). We start with a general Landau–de Gennes type expansion [2,40,49,50] of the elastic free energy density $f_e(\mathbf{r})$ in terms of a tensor nematic order parameter $\mathbf{Q}_{ij}$:

$$\begin{aligned} f_e(\mathbf{r}) = & L^{(1)}\mathbf{Q}_{ij,ij} + L_1^{(2)}\mathbf{Q}_{jk,i}\mathbf{Q}_{jk,i} + L_2^{(2)}\mathbf{Q}_{ij,i}\mathbf{Q}_{kj,k} + L_3^{(2)}\mathbf{Q}_{jk,i}\mathbf{Q}_{ik,j} \\ & + L_5^{(2)}\mathbf{Q}_{ik,ij}\mathbf{Q}_{jk} + L_6^{(2)}\mathbf{Q}_{jk,ii}\mathbf{Q}_{jk} L_1^{(3)}\mathbf{Q}_{ij}\mathbf{Q}_{ij,k}\mathbf{Q}_{kl,l} + L_2^{(3)}\mathbf{Q}_{ij}\mathbf{Q}_{ik,j}\mathbf{Q}_{kl,l} \\ & + L_3^{(3)}\mathbf{Q}_{ij}\mathbf{Q}_{ik,k}\mathbf{Q}_{jl,l} L_4^{(3)}\mathbf{Q}_{i,}\mathbf{Q}_{ik,l}\mathbf{Q}_{jk,l} + L_5^{(3)}\mathbf{Q}_{ij}\mathbf{Q}_{ik,l}\mathbf{Q}_{jl,k} + L_6^{(3)}\mathbf{Q}_{ij}\mathbf{Q}_{ik,l}\mathbf{Q}_{kl,j} + \cdots , \end{aligned} \tag{A1}$$

where $L_i^{(j)}$ are temperature independent elastic constants. In the case of a uniaxial nematic phase $\mathbf{Q}_{ij}$ can be expressed as [49]

$$\mathbf{Q}_{ij} = \frac{S}{2}(3n_i n_j - \delta_{ij}) . \tag{A2}$$

Here n_i denotes the ith director field component and S is the uniaxial orientational order parameter. In the case of a constant value of S the expression (A1) transforms to

$$\begin{aligned} f_e(\mathbf{r}) = & \frac{K_{11}}{2}(\mathrm{div}\mathbf{n})^2 + \frac{K_{22}}{2}(\mathbf{n}\cdot\mathrm{curl}\mathbf{n})^2 + \frac{K_{33}}{2}(\mathbf{n}\times\mathrm{curl}\mathbf{n})^2 \\ & - \frac{K_{24}}{2}(\mathbf{n}\times\mathrm{curl}\mathbf{n} + \mathbf{n}\,\mathrm{div}\mathbf{n})\cdot\nu\delta(\mathbf{r}-\mathbf{R}) \\ & + K_{13}(\mathbf{n}\,\mathrm{div}\mathbf{n})\cdot\nu\delta(\mathbf{r}-\mathbf{R}) . \end{aligned} \tag{A3}$$

The elastic constants in Eqs. (A1) and (A3) are related via

$$\begin{aligned} K_{11} = & \frac{9S^2}{2}(2L_1^{(2)} + L_2^{(2)} + L_3^{(3)} - L_5^{(2)} - 2L_6^{(2)}) \\ & + \tfrac{9}{4}S^3(-L_2^{(3)} + 2L_3^{(3)} + L_4^{(3)} + 2L_5^{(3)} - L_6^{(3)}) , \end{aligned} \tag{A3a}$$

$$K_{22} = 9S^2(L_1^{(2)} - L_6^{(2)}) + \frac{9S^3}{4}L_4^{(3)} , \tag{A3b}$$

$$\begin{aligned} K_{33} = & \frac{9S^2}{2}(2L_1^{(2)} + L_2^{(2)} + L_3^{(2)} - L_5^{(2)} - 2L_6^{(2)}) \\ & + \frac{9S^3}{4}(2L_2^{(3)} - L_3^{(3)} + L_4^{(3)} - L_5^{(3)} + 2L_6^{(3)}) , \end{aligned} \tag{A3c}$$

$$\begin{aligned} K_{24} = & 3SL^{(1)} + \frac{9S^2}{2}(2L_1^{(2)} + L_3^{(2)} - \tfrac{1}{3}L_5^{(2)} - 2L_6^{(2)}) \\ & + \frac{9S^3}{2}(L_4^{(3)} + 2L_5^{(3)} - L_6^{(3)}) , \end{aligned} \tag{A3d}$$

$$K_{13} = 3SL^{(1)} + \frac{3S^2}{4}L_5^{(2)} . \tag{A3e}$$

APPENDIX B: DERIVATION OF THE SURFACE BOUNDARY CONDITION

In the following we derive Eq. (3b), which determines the surface boundary condition for the escaped radial structures. We originate from dimensionless free energy given in Eq. (2). Using the parametrization $\mathbf{n}(\rho,z) = -\mathbf{e}_\rho \sin\theta + \mathbf{e}_z \cos\theta$ the dimensionless free energy G per unit cylinder length is

$$\begin{aligned} G = & \frac{2\pi}{1}\left\{ \int_0^1 \rho\, d\rho \int_0^1 dz\, g_e\left[\theta, \frac{\partial\theta}{\partial\rho}, \frac{\partial\theta}{\partial z}\right] \right. \\ & \left. + \int_0^1 dz \left[g_{24}\left[\theta, \frac{\partial\theta}{\partial z}\right] + g_a(\theta) \right]_{\rho=1} \right\} . \end{aligned} \tag{B1}$$

Here $l = L_{\mathrm{PD}}/R$ for ERPD and $l = L/R$ for the ER structure. The elastic (g_e), "surface" elastic (g_{24}), and anchoring (g_a) contribution are expressed as

$$\begin{aligned} g_e = & \frac{1}{2}\left[\left[\frac{\partial\theta}{\partial\rho}\right]^2 (\cos^2\theta + a_{33}\sin^2\theta) + \left[\frac{\partial\theta}{\partial z}\right]^2 (\sin^2\theta + a_{33}\cos^2\theta) \right. \\ & \left. + \frac{\partial\theta}{\partial\rho}\frac{\sin(2\theta)}{\rho} + \frac{\partial\theta}{\partial z}\frac{2\sin^2\theta}{\rho} + \frac{\sin^2\theta}{\rho^2} + (1-a_{33})\sin(2\theta)\frac{\partial\theta\partial\theta}{\partial\rho\partial z} \right] , \end{aligned} \tag{B1a}$$

$$g_{24}=-\frac{a_{24}}{2}\left[\frac{\sin^2\theta}{\rho}+\frac{\partial\theta}{\partial z}\right], \tag{B1b}$$

$$g_a=\frac{\mu}{2}\cos^2\theta\ . \tag{B1c}$$

We see that g_{24} depends also on $\partial\theta/\partial z$. This derivative is zero in the ER structure where $\theta=\theta(\rho)$. Note that g_{24} has a particularly simple structure because of the cylindrical symmetry [the surface normal in Eq. (1) is along $\mathbf{e}_\rho$]. In the following we will see that for such a case $\partial\theta/\partial z$ does not enter the surface Euler-Lagrange equation describing the condition at $\rho=1$.

We carry out the variational procedure

$$\begin{aligned}\delta G/(2\pi/1)=&\int_0^1\rho\,d\rho\int_0^1 dz\left[\frac{\partial g_e}{\partial\theta}\delta\theta+\frac{\partial g_e}{\partial\left[\frac{\partial\theta}{\partial\rho}\right]}\delta\left[\frac{\partial\theta}{\partial\rho}\right]+\frac{\partial g_e}{\partial\left[\frac{\partial\theta}{\partial z}\right]}\delta\left[\frac{\partial\theta}{\partial z}\right]\right]\\&+\int_0^1 dz\left[\frac{\partial g_{24}}{\partial\theta}\delta\theta+\frac{\partial g_{24}}{\partial\left[\frac{\partial\theta}{\partial z}\right]}\delta\left[\frac{\partial\theta}{\partial z}\right]+\frac{\partial g_a}{\partial\theta}\delta\theta\right]_{\rho=1}+\cdots,\\=&\int_0^1\rho\,d\rho\int_0^1 dz\left[\frac{\partial g_e}{\partial\theta}-\frac{1\partial}{\rho\partial_\rho}\left[\rho\frac{\partial g_e}{\partial\left[\frac{\partial\theta}{\partial\rho}\right]}\right]-\frac{\partial}{\partial z}\left[\frac{\partial g_e}{\partial\left[\frac{\partial\theta}{\partial z}\right]}\right]\right]\delta\theta\\&+\int_0^1 dz\left[\frac{\partial g_{24}}{\partial\theta}-\frac{\partial}{\partial z}\left[\frac{\partial g_{24}}{\partial\left[\frac{\partial\theta}{\partial z}\right]}\right]+\frac{\partial g_a}{\partial\theta}+\rho\frac{\partial g_e}{\partial\left[\frac{\partial\theta}{\partial\rho}\right]}\right]_{\rho=1}\delta\theta+\cdots\ .\end{aligned} \tag{B2}$$

In Eq. (B2) the first term determines the bulk Euler-Lagrange equation and the second term the surface equation at the lateral wall ($\rho=1$) of the cylinder. The remaining terms, not written in Eq. (B2), describe boundary conditions at other nematic phase boundaries. In numerical calculations we enforce the ERPD director field by setting the planar radial structure at $z=0,1$ and the ER director field is homogeneous in the z direction.

Thus the surface equation at $\rho=1$ is

$$\frac{\partial g_{24}}{\partial\theta}-\frac{\partial}{\partial z}\left[\frac{\partial g_{24}}{\partial\left[\frac{\partial\theta}{\partial z}\right]}\right]+\frac{\partial g_a}{\partial\theta}+\frac{\partial g_e}{\partial\left[\frac{\partial\theta}{\partial\rho}\right]}=0\ . \tag{B3}$$

Taking into account Eqs. (B1) we derive Eq. (3b). Although in the ERPD structure $\partial\theta/\partial z\neq 0$, we see that this derivative does not enter Eq. (3b). It is important to mention that in the general case the tangential (with respect to the surface normal) derivatives are present in the K_{24} free energy contribution and do not cause any mathematical problems. In contrast the normal derivatives, which are present only in the K_{13} contribution, introduce mathematical difficulties. There are currently two controversial theories [34,43] dealing with this problem.

APPENDIX C: FREE ENERGY OF THE PR STRUCTURE TAKING INTO ACCOUNT THE $S(\mathbf{r})$ VARIATION

In order to evaluate the free energy of the PR structure allowing a $S(\mathbf{r})$ variation we express the free energy density as [12,49]

$$\begin{aligned}f(\mathbf{r})=&\frac{A(T-T_*)}{2}S^2-\frac{B}{3}S^3+\frac{C}{4}S^4\\&+\frac{KS^2}{2}[(\mathrm{div}\mathbf{n})^2+(\mathrm{curl}\mathbf{n})^2]\\&+\frac{K}{6}(\mathrm{grad}S)^2-WS\delta(\mathbf{r}-\mathbf{R})\ .\end{aligned} \tag{C1}$$

Here A, T_*, B, C are material constants, $K=K_{11}=K_{22}=K_{33}$, W represents the surface wetting strength [12], and T is temperature. For the sake of simplicity we have discarded a K_{13} and K_{24} term in Eq. (C1).

In the PR structure the director field is given by $\mathbf{n}(\mathbf{r})=\mathbf{e}_\rho$, yielding

$$\begin{aligned}g(\rho)=f/(K/R^2)=&\frac{a}{2}S^2-\frac{bS^3}{3}+\frac{c}{4}S^4+\frac{S^2}{2\rho^2}\\&+\frac{1}{6}\left[\frac{dS}{d\rho}\right]^2\\&-qS\delta(\rho-1)\ .\end{aligned} \tag{C2}$$

In Eq. (C2) we have introduced the dimensionless parameters $a=A(T-T_*)R^2/K$, $b=BR^2/K$, $c=CR^2/K$, $q=WR/K$. The minimization of $g(\rho)$ yields the bulk Euler-Lagrange equation

$$\frac{dS^2}{d\rho^2}+\frac{1}{\rho}\frac{dS}{d\rho}-\frac{3}{\rho^2}(aS-bS^2+cS^3)-\frac{3S}{\rho^2}=0\ , \tag{C3a}$$

with boundary conditions

$$\left[\frac{dS}{d\rho}\right](\rho=1)=3q\ ,\quad S(\rho=0)=0\ . \tag{C3b}$$

We solve Eqs. (C3) numerically and from the obtained $S(\rho)$ dependence evaluate the dimensionless free energy per unit cylinder length

$$G=\int_0^1 g[s(\rho)]\rho\,d\rho\ . \tag{C4}$$

In calculations performed in this article we assume a constant value of $S=S_b$, where S_b describes the bulk nematic orientational order parameter. To avoid singularities at defect sites in this approximation we have introduced an isotropic core surrounding the defect. The core radius ρ_c is approximately obtained from the condition [2] $aS_b^2/2-bS_b^3/3+cS_b^4/4+S_b^2/(2\rho_c^2)=0$, yielding

$$\rho_c=\left[-2\left[\frac{a}{2}-\frac{bS_b}{3}+\frac{cS_b^2}{4}\right]\right]^{-1/2}\ . \tag{C5a}$$

Here

$$S_b=(b+\sqrt{b^2-4ac}\,)/(2c) \tag{C5b}$$

minimizes the homogeneous part of $g(\rho)$. Taking this into account we get for the PR director field

$$G=\int_{\rho_c}^1 g(\rho)\rho\,d\rho\approx\frac{1}{2}\left[\frac{a}{2}S_b^2-\frac{b}{3}S_b^3+\frac{c}{4}S_b^4-S_b^2\ln(\rho_c)\right]\ . \tag{C6}$$

For supramicrometer droplets a difference between a value of G evaluated from Eqs. (C6) and (C4) is, for typical values of nematic liquid crystal material constants, negligible (below 1%).

APPENDIX D: SADDLE-SPLAY CONTRIBUTION IN A BIAXIAL NEMATIC PHASE

Our aim is to show that the saddle-splay elastic constant does not influence planar (two dimensional) nematic director structures. In planar structures nematic molecules are restricted to lie in one plane. We originate from the Landau–de Gennes free energy expression in terms of the tensor nematic order parameter [49] $\mathbf{Q}(\mathbf{r})$:

$$f(\mathbf{r})=\tfrac{1}{2}L_1\mathbf{Q}(\mathbf{r})_{ij,k}\mathbf{Q}(\mathbf{r})_{ij,k}\ . \tag{D1}$$

The quantity L_1 denotes the temperature independent nematic elastic constant. This model is for a uniaxial nematic liquid crystal and spatially independent nematic order parameter S equivalent to the Frank free energy expression in the approximation of equal Frank nematic elastic constants. Indices i,j,k in Eq. (D1) denote tensor components in the Cartesian coordinate system (x_1,x_2,x_3), $\mathbf{Q}_{ij,k}=\partial\mathbf{Q}_{ij}/\partial x_k$, and the summation over the repeated indices is assumed. The nematic order parameter tensor field $\mathbf{Q}(\mathbf{r})$ can be expressed as [50]

$$\mathbf{Q}_{ij}=\frac{S(\mathbf{r})}{2}[3n_i(\mathbf{r})n_j(\mathbf{r})-\delta_{ij}]+T(\mathbf{r})[l_i(\mathbf{r})l_j(\mathbf{r})-m_i(\mathbf{r})m_j(\mathbf{r})]\ . \tag{D2}$$

Here δ_{ij} stands for the Kronecker tensor. Orthogonal unit vectors (directors) $\mathbf{n}(\mathbf{r})$, $\mathbf{m}(\mathbf{r})$, $\mathbf{l}(\mathbf{r})$ define the local coordinate system within which $\mathbf{Q}(\mathbf{r})$ is diagonal. The quantities $S(\mathbf{r}),T(\mathbf{r})$ are the uniaxial and biaxial scalar nematic order parameters, respectively. In large cylinders ($R>1$ μm) one can to a good approximation neglect spatial variations of scalar order parameters. Therefore we set $S(\mathbf{r})=S_b$, $T(\mathbf{r})=T_b$, where the index b denotes a spatially independent bulk order parameter value. With this in mind and taking into account $\mathbf{l}=\mathbf{m}\times\mathbf{n}$, $m_im_{i,k}=n_in_{i,k}=n_im_i=0$, it follows that

$$\mathbf{Q}_{ij,k}\mathbf{Q}_{ij,k}=\frac{9}{2}\left[S_b-\frac{2T_b}{3}\right]^2 n_{i,k}n_{i,k}+8T_b^2m_{i,k}m_{i,k}\ . \tag{D3}$$

Next we recall the equality [49]

$$a_{i,j}a_{i,j}=(\nabla\cdot\mathbf{a})^2+(\mathbf{a}\cdot\nabla\times\mathbf{a})^2+(\mathbf{a}\times\nabla\times\mathbf{a})^2-\nabla\cdot(\mathbf{a}\nabla\cdot\mathbf{a}+\mathbf{a}\times\nabla\mathbf{a})\ , \tag{D4}$$

where $\mathbf{a}$ is an arbitrary unit director field. Taking this into account we get

$$\mathbf{Q}_{ij,k}\mathbf{Q}_{ij,k}=\frac{9}{2}\left[S_b-\frac{2T_b}{3}\right]^2[(\nabla\cdot\mathbf{n})^2+(\mathbf{n}\cdot\nabla\times\mathbf{n})^2+(\mathbf{n}\times\nabla\times\mathbf{n})^2]+8T_b^2[(\nabla\cdot\mathbf{m})^2+(\mathbf{m}\cdot\nabla\times\mathbf{m})^2+(\mathbf{m}\times\nabla\times\mathbf{m})^2]$$
$$-\frac{9}{2}\left[S_b-\frac{2T_b}{3}\right]^2\nabla\cdot(\mathbf{n}\nabla\cdot\mathbf{n}+\mathbf{n}\times\nabla\mathbf{n})-8T_b^2\nabla\cdot(\mathbf{m}\nabla\cdot\mathbf{m}+\mathbf{m}\times\nabla\mathbf{m})\ . \tag{D5}$$

The last two terms in Eq. (D5) present the saddle-splay contribution to the elastic free energy. But if any unit vector field $\mathbf{a}$ is restricted to a plane [1] it holds,

$$\nabla\cdot(\mathbf{a}\nabla\cdot\mathbf{a}+\mathbf{a}\times\nabla\mathbf{a})=0\ . \tag{D6}$$

Therefore the saddle-splay term does not contribute to planar structures even in the biaxial case.

[1] D. W. Allender, G. P. Crawford, and J. W. Doane, Phys. Rev. Lett. **67**, 1442 (1991); G. P. Crawford, D. W. Allender, and J. W. Doane, Phys. Rev. A **45**, 8693 (1992).
[2] S. Kralj and S. Žumer, Phys. Rev. A **45**, 2461 (1992).
[3] H. S. Kitzerov, Liq. Cryst. **16**, 1 (1994).
[4] S. Candau, P. LeRoy, and F. Debeauvais, Mol. Cryst. Liq. Cryst. **23**, 283 (1973).
[5] G. E. Volovik and O. D. Lavrentovich, Zh. Eksp. Teor. Fiz. **85**, 1997 (1983) [Sov. Phys. JETP **58**, 1159 (1983)].
[6] V. G. Bodnar, O. D. Lavrentovich, and V. M. Pergamenshchik, Zh. Eksp. Teor. Fiz. **101**, 111 (1992) [Sov. Phys. JETP **47**, 61 (1992)].
[7] B. J. Liang and S. H. Chen, Jpn. Appl. Phys. **30**, L1955 (1991); S. H. Chen and B. J. Liang, Appl. Phys. Lett. **59**, 1173 (1991).
[8] J. W. Doane, N. A. Vaz, B. G. Wu, and S. Žumer, Appl. Phys. Lett. **48**, 269 (1986).
[9] S. Žumer and J. W. Doane, Phys. Rev. A **34**, 3373 (1986).
[10] A. Sharkowski, G. P. Crawford, S. Žumer, and J. W. Doane, J. Appl. Phys. **73**, 7280 (1993).
[11] R. D. Polak, G. P. Crawford, B. C. Kostival, J. W. Doane, and S. Žumer, Phys. Rev. E **49**, R9078 (1994).
[12] P. Sheng, Phys. Rev. A **3**, 1610 (1982).
[13] A. Golemme, S. Žumer, D. W. Allender, and J. W. Doane, Phys. Rev. Lett. **61**, 2937 (1988).
[14] S. Kralj, S. Žumer, and D. W. Allender, Phys. Rev. A **34**, 2943 (1991).
[15] T. Bellini, N. A. Clark, C. F. Muzny, L. Wu, C. W. Garland, D. W. Schaefer, and B. J. Oliver, Phys. Rev. Lett. **69**, 788 (1992).
[16] G. S. Iannacchione, G. P. Crawford, S. Žumer, J. W. Doane, and D. Finotello, Phys. Rev. Lett. **71**, 2595 (1993).
[17] B. Jerome, Rep. Prog. Phys. **54**, 351 (1991), and references therein.
[18] M. Kléman, *Points, Lines and Walls* (Wiley, Chichester, 1983).
[19] P. G. de Gennes, Solid State Commun. **10**, 753 (1972).
[20] N. D. Mermin, Rev. Mod. Phys. **51**, 591 (1976).
[21] N. Schopohl and T. J. Sluckin, J. Phys. **49**, 1097 (1988).
[22] D. N. Spergel and N. G. Turok, Sci. Am. **3** (3), 36 (1992).
[23] P. G. de Gennes, *The Physics of Liquid Crystals* (Oxford, London, 1974).
[24] G. Vertogen and W. H. de Jeu, *Thermotropic Liquid Crystals* (Springer-Verlag, Berlin, 1988).
[25] E. Dzyaloshinskii, Zh. Eskp. Teor. Fiz. **31**, 773 (1970) [Sov. Phys. JETP **33**, 733 (1970)].
[26] P. E. Cladis and M. Kléman, J. Phys. **33**, 591 (1972).
[27] R. B. Meyer, Philos. Mag. **27**, 405 (1973).
[28] E. Williams, P. E. Cladis, and M. Kléman, Mol. Cryst. Liq. Cryst. **21**, 355 (1973).
[29] I. Vilfan, M. Vilfan, and S. Žumer, Phys. Rev. A **43**, 6875 (1991).
[30] G. P. Crawford, M. Vilfan, J. W. Doane, and I. Vilfan, Phys. Rev. A **43**, 835 (1991).
[31] R. J. O. Crawford, G. P. Crawford, J. W. Doane, S. Žumer, M. Vilfan, and I. Vilfan, Phys. Rev. E **48**, 1998 (1993).
[32] S. Kralj and S. Žumer, Liq. Cryst. **15**, 521 (1993).
[33] G. Barbero and A. Strigazzi, J. Phys. Lett. **45**, 857 (1984).
[34] V. M. Pergamenshchik, Phys. Rev. E **48**, 1254 (1993).
[35] G. Barbero and G. Durand, Phys. Rev. E **48**, 1942 (1993).
[36] O. D. Lavrentovich and V. M. Pergamenshchik, Phys. Rev. Lett. **73**, 979 (1994).
[37] F. C. Frank, Discuss. Faraday Soc. **25**, 19 (1958).
[38] A. Saupe, J. Chem. Phys. **75**, 5118 (1981).
[39] A. Rapini and M. Papoular, J. Phys. (Paris) Colloq. **30**, C4-54 (1969).
[40] A. I. Alexe-Ionescu, G. Barbero, and G. Durand, J. Phys. (France) II **3**, 1247 (1993).
[41] P. I. C. Teixeira, V. M. Pergamenshchik, and T. J. Sluckin, Mol. Phys. **80**, 1338 (1993).
[42] J. Nehring and A. Saupe, J. Chem. Phys. **54**, 337 (1971); **56**, 5527 (1972).
[43] C. Oldano and G. Barbero, J. Phys. (Paris) Lett. **46**, L451 (1984); G. Barbero and C. Oldano, Nuovo Cimento D **6**, 479 (1985).
[44] W. H. Press, B. P. Flannery, S. A. Teukolsky, and W. T. Vetterling, *Numerical Recipes* (Cambridge University Press, Cambridge, England, 1986), Chap. 17.
[45] S. Žumer and S. Kralj, Liq. Cryst. **12**, 613 (1992).
[46] J. Bezič and S. Žumer, Liq. Cryst. **14**, 1695 (1993).
[47] J. Liu and A. Saupe (unpublished).
[48] S. Faetti, Phys. Rev. E **49**, 4129 (1994).
[49] E. B. Priestley, P. J. Wojtowitz, and P. Sheng, *Introduction to Liquid Crystals* (Plenum, New York, 1975), p. 143.
[50] D. Monselesan and H. R. Trebin, Phys. Status Solidi **155**, 349 (1989).